PROCEEDINGS B

royalsocietypublishing.org/journal/rspb

Research

Cite this article: Prondvai E, Horváth K, Price SWT, Gutowski O, Beale AM. 2026 United by chewing: Hunter-Schreger band-like pattern and wavy enamel in a fossil crocodile suggest functional convergence with mammals and dinosaurs. *Proc. R. Soc. B* **293**: 20251992. https://doi.org/10.1098/rspb.2025.1992

Received: 3 August 2025
Accepted: 10 December 2025

Subject Category:
Palaeobiology

Subject Areas:
palaeontology, evolution

Keywords:
Hunter-Schreger bands, crocodilian tooth enamel, *Iharkutosuchus*, wavy enamel, XRD-CT, chewing-related adaptation, convergent evolution, herbivorous crocodile

Author for correspondence:
Edina Prondvai
e-mail: edina.prondvai@gmail.com

Electronic supplementary material is available online at https://doi.org/10.6084/m9.figshare.c.8210474.

THE ROYAL SOCIETY PUBLISHING

United by chewing: Hunter-Schreger band-like pattern and wavy enamel in a fossil crocodile suggest functional convergence with mammals and dinosaurs

Edina Prondvai[1,2], Krisztián Horváth[3,4], Stephen WT Price[5], Olof Gutowski[6] and Andrew M. Beale[7,8]

[1]School of Life Sciences, University of Warwick Faculty of Science, Coventry CV4 7AL, UK
[2]School of Geography, Earth and Environmental Sciences, University of Birmingham Edgbaston Campus, Birmingham B15 2TT, UK
[3]Department of Social and Economic Geography, and [4]Department of Palaeontology, Eötvös Loránd University Faculty of Science, Budapest 1117, Hungary
[5]Finden Ltd, Oxford OX11 0QX, UK
[6]Deutsches Elektronen-Synchrotron DESY, Hamburg 22607, Germany
[7]Department of Chemistry, University College London, London WC1E 6BT, UK
[8]R92, Research Complex at Harwell, Didcot OX11 0FA, UK

EP, 0000-0002-1284-8311; SWTP, 0000-0002-5329-4351; AMB, 0000-0002-0923-1433

Tooth enamel of most mammals shows alternating light and dark bands, called Hunter-Schreger bands (HSB), in longitudinal sections caused by decussating bundles of prisms, the unit building blocks of mammalian enamel. HSB are thought to increase resistance to abrasive food and mitigate crack propagation and hence are considered a mammalian adaptation to high-efficiency mastication. Using traditional microscopy techniques as well as X-ray diffraction computed tomography (XRD-CT), here we report for the first time the presence of HSB-like features in the tooth enamel of a non-mammalian amniote, *Iharkutosuchus*, an extinct herbivorous crocodile with strong heterodonty and a unique chewing mechanism. XRD-CT showed that the enigmatic HSB-like pattern in *Iharkutosuchus* enamel, which lacks mammal-like decussating prisms, has a purely crystallographic origin. *Iharkutosuchus* teeth also exhibit wavy enamel, a well-known structure in herbivorous ornithopod dinosaurs with shearing-type mastication. The unexpected finding of both enamel features in this herbivorous crocodile speaks for their role in high-efficiency chewing. However, the profoundly different structural background of mammalian and crocodilian HSB demonstrated here and the phylogenetic distribution of both HSB and wavy enamel indicate nanostructure-scale convergences, highlighting the importance of mastication-related challenges in driving dental evolution of amniotes.

1. Introduction

From the well-organized and repeated decussation pattern of bundles of enamel prisms, the unit building blocks of mammalian tooth enamel, emerge an optical feature referred to as Hunter-Schreger bands (HSB). HSB are known to appear in the longitudinal section of most mammalian teeth as alternating light and dark bands in the enamel under cross-polarized light [1–4]. It has long been suggested that the criss-crossing bundles of prisms in HSB, appearing distinctly under scanning electron microscope (SEM), limit

the propagation of fractures [5–8] and reduce mastication-related enamel abrasion [9]. Thus, the presence of HSB is generally considered indicative of an animal's chewing performance. Some evolutionary studies even implied that the polyphyletic appearance of HSB has driven the diversification of Cenozoic herbivore and carnivore mammals by expanding their range of diet [6,10]. Apart from two studies reporting its presence in some fossil sauropsid taxa without providing visual evidence [11,12], HSB have so far only been demonstrated sufficiently in diverse mammalian species. Consequently, they are thought of as primarily a mammalian feature [13].

The functional importance of HSB is undisputedly connected with the capability of chewing, in which food is pre-processed orally by the occluding teeth of the upper and lower jaws. The emergence of mastication with dental occlusion in the evolution of vertebrates is thought to be associated with a herbivorous diet [14,15]. Among extant vertebrates, oral food processing by active chewing only occurs in mammals. However, it was phylogenetically much more widespread among extinct amniotes, such as non-mammalian synapsids [15], ornithischian dinosaurs [16–18], placodontian marine reptiles [19,20] and even some intriguing crocodilians [21,22]. A special representative of the latter group is *Iharkutosuchus makadii*, a small-bodied (approx. 1 m long), Late Cretaceous semiaquatic hylaeochampsid crocodile described from the Santonian-aged (approx. 85 Ma) Csehbánya Formation (Iharkút, Bakony Mountain, Hungary) based on one nearly complete and multiple partial skulls with *in situ* preserved teeth and plenty of isolated teeth [23]. This peculiar species exhibits a short snout (approx. 11 cm skull length) with heterodont dentition composed of incisiviform and multicusped premolariform and molariform teeth (figure 1A,B). Based on extensive comparative anatomical and tooth wear analysis, *Iharkutosuchus* was a predominantly herbivorous crocodile with a unique chewing mechanism involving predominantly lateromedial jaw movements with a slight mesiodistal component [22–25].

Using traditional cross-polarized light microscopic (c-PLM) and SEM visualization techniques as well as X-ray diffraction computed tomography (XRD-CT) applied here for the first time in the comparative context of extant and sympatric fossil crocodilian teeth, we report the presence of HSB-like patterns in the tooth enamel of *Iharkutosuchus*. While c-PLM provided the first visual clue, XRD-CT could explain the origin of this feature by providing evidence of its crystallographic background that is fundamentally different from the alternating prisms seen in mammalian HSB under SEM. Besides the HSB-like pattern, we also show the presence of wavy enamel, a structure well-known and described in the dental histology of the herbivorous ornithopod dinosaurs and associated with a shearing type of chewing [26–31]. The differing structural origin of HSB between *Iharkutosuchus* and mammals, and the phylogenetic distribution of both HSB and wavy enamel indicate evolutionary convergence and a functional importance related to high-efficiency mastication. This study is the first to clearly demonstrate and explain HSB-like enamel features in a non-mammalian amniote. We also highlight the indispensability of X-ray-based imaging techniques, such as XRD-CT, as non-destructive tools to decipher hidden crystallographic features with potential functional implications in fossil teeth.

2. Methods

(a) Investigated taxa and tooth material

Fifteen isolated *Iharkutosuchus* teeth representing three different morphotypes were investigated in this study: four incisiviform, three premolariform and seven molariform teeth (figure 1A,B; electronic supplementary material, table S1). To provide comparative context for the interpretation of their unique enamel characteristics, we also selected isolated posterior teeth of a further three extinct mesoeucrocodylian groups as well as an anterior and a posterior tooth of an extant American alligator (*Alligator mississippiensis*) (electronic supplementary material, figure S1). All isolated fossil crocodilian teeth studied here have been recovered from the same locality in Iharkút, the Santonian-aged Csehbánya Formation, Bakony Mts, Hungary, and are curated in the Hungarian Natural History Museum (HNHM). These sympatric fossil taxa are representatives of the enigmatic allodaposuchid and theriosuchid crocodiles and the genus *Doratodon* [32] (electronic supplementary material, figure S1). Here, we mostly focused on the semiaquatic allodaposuchid crocodilians because, unlike the terrestrial *Doratodon*, they shared the same fluvial habitat with *Iharkutosuchus* and thereby were exposed to the same taphonomy and diagenetic conditions during fossilization [33]. At the same time, as the dentition and assumed diet of allodaposuchids were similar to those of modern crocodiles [34–36], their teeth provided the best baseline comparison with *Iharkutosuchus* teeth to contrast potentially diet-related enamel patterns. On the other hand, teeth positively assignable to the similarly semiaquatic theriosuchid crocodilians are comparatively rare in this locality, and hence our study was limited to a single theriosuchid posterior tooth. The extant American alligator anterior and posterior teeth have been extracted from a skull specimen commercially acquired from the Atlantic Coral Enterprise, Inc. in St. Augustine, Florida, USA.

Whereas the *Iharkutosuchus* and allodaposuchid teeth were subjected to all imaging and analytical techniques presented in this study, including PLM, SEM and XRD-CT, theriosuchid and *Doratodon* teeth were investigated only as petrographic sections with PLM. The extant alligator teeth were characterized by XRD-CT only, owing to the numerous PLM and SEM images and descriptions available in the literature for comparison [e.g. 26,37–39]. *Iharkutosuchus* tooth morphology and general enamel microstructure have previously been described [22,23,25]. For technical information on the selected teeth, including the number of tooth specimens investigated in each group, catalogue numbers and section planes, see electronic supplementary material, table S1.

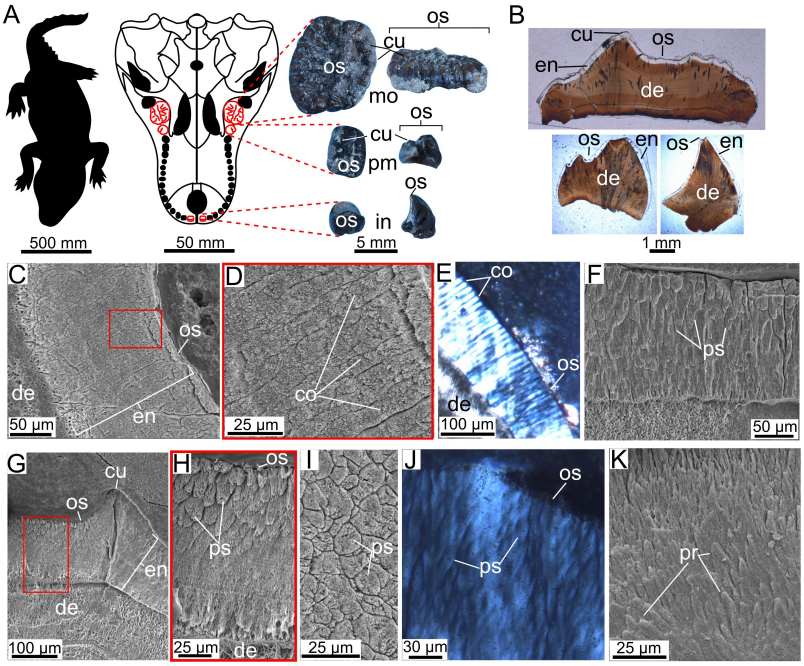

Figure 1. General anatomical and dentition characteristics of the heterodont hylaeochampsid crocodile, *Iharkutosuchus*. (A) Reconstructed body silhouette and skull of *Iharkutosuchus* in ventral view with the studied incisiviform (in), premolariform (pm) and molariform (mo) teeth highlighted in red, and the actual tooth specimens magnified (incisiviform and molariform in occlusal and medial views, premolariform in occlusal and mesial views). (B) Thin sections of teeth cut in mesiodistal (= longitudinal) plane. (C,D,E) Columnar microstructure of the enamel (en) demonstrated in a molariform tooth in SEM (C) and (D) and cross-polarized light microscopic (c-PLM) (E) images. The red rectangle in (C) indicates the magnified region in (D). (F–J) Prism-like structures (ps) are shown in molariform teeth in SEM (F)–(I) and c-PLM (J) images (I in cross-section). Red rectangle in (G) indicates magnified region in (H). (K) Mammalian prismatic enamel in a rodent molar tooth for comparison. Further abbreviations: cu, cusps; co, columns; de, dentin; os, occlusal surface; pr, enamel prisms.

(b) Sample preparation, visualization and analytical techniques

(i) Polarized light microscopy (PLM)

Fossil teeth were embedded in Araldite 2020 epoxy resin, and petrographic ground sections in longitudinal (mesiodistal and labiolingual) and transverse planes prepared following the method outlined in Prondvai *et al*. [40]. Histological and image analyses were performed using a Nikon ECLIPSE LV100 POL polarized light microscope, QImaging Micro Publisher 5.0 digital CCD camera, and Image-Pro Insight 8.0 software (Media Cybernetics).

(ii) Scanning electron microscopy (SEM)

For the SEM analysis, the resin-embedded *Iharkutosuchus* and allodaposuchid teeth were cut in various planes, ground, their etched surfaces coated with a 5 nm gold–palladium layer by an XC7620 Mini Sputter Coater and analysed using a Hitachi S-2360N SEM at the Department of Botany, HNHM. Images were taken at 15–20 kV from 5 to 9 mm distance using Everhart-Thornley detector. With the same specimen preparation but applying 5 nm carbon-coating and using a FEI Quanta 3D FEG SEM for the analysis of tooth microstructure, another SEM analysis was conducted at the Research and Instrument Core Facility, Faculty of Science, Eötvös Loránd University, Hungary.

(iii) X-ray diffraction computed tomography (XRD-CT)

Hydroxyapatite (HAP), the main mineral constituent of enamel, preserves well in fossils and is thought to largely reflect the original crystallographic arrangements, especially crystallite orientations [41]. This is particularly true of tooth enamel, which has high crystallinity and low organic content [42]. Hence, application of X-ray diffraction-based methods can reveal characteristics that are hidden from PLM and SEM techniques traditionally used in descriptive studies of fossil teeth. For the first time in fossil teeth, we apply non-destructive XRD-CT, a cross-disciplinary approach that has already been successfully used in imaging the crystalline structure of human teeth [43,44], to decipher the structural background of the HSB-like pattern in *Iharkutosuchus* teeth.

XRD-CT is a focused pencil-beam computed tomography method in which the signal corresponds to differences in the diffracted intensity of X-rays [45], enabling spatial resolution of chemical species of similar density or low absorption cross-section. It informs about crystallinity (i.e. level of structural order reflecting the density of HAP packing), crystallite size and unit cell parameters, including size and orientation along the main axes. For XRD-CT-based comparison, we selected an intact premolariform and a molariform tooth from *Iharkutosuchus* with well-preserved ridges, cusps and general 3D morphology,

an isolated posterior allodaposuchid tooth and a posterior and an anterior tooth of an extant American alligator (electronic supplementary material, table S1).

XRD-CT data were measured using beamline P07 (EH2) at PETRA III, DESY, Hamburg. The beam energy was 73.4 keV (0.169 Å), focused to 2 × 20 µm (vertical × horizontal). Data were collected at 500 Hz using an Eiger X 4M hybrid pixel detector at 900 mm sample–detector distance and calibrated using a CeO_2 reference standard (NIST, 99.9%, < 5 micron). The samples were mounted atop a goniometer with a horizontal rotation axis and oriented such that the measurement followed a longitudinal slice down the tooth. The samples were scanned with continuous translation (vertical) steps of 4 µm in a zig-zag configuration and with a 0–360° rotation range using 1000 steps of 0.36°. A beam monitor diode was used for sample absorption correction.

The raw 2D diffraction images were integrated using PyFAI [46]. Sinogram alignment, absorption correction and reconstruction with filtered back-projection were performed using in-house Matlab scripts. The final reconstructed images have a pixel size of 4 × 4 µm. Reconstructed XRD-CT datasets were masked to exclude the dentin, after which Rietveld refinement was applied using Beamstop [47] over the range of 15–68° (when scaled to λ = 1.5406 Å) and Topas V7 utilized [48] on the masked datasets using the hydroxylapatite structure (ICSD 131599), with +/–1 % min/max limits on the reported unit cell parameters [a = 9.42, c = 6.88]. For further explanation on the Rietveld analysis, see Electronic Supplementary Information.

In addition to the Rietveld analysis, two peaks of interest were fitted with Gaussian profiles: the 002 and 300 reflections (3.436 Å and 2.719 Å d-spacing). These peaks were chosen as unique reflections representing the c- and a-axes of the unit cell and providing additional information on the relative crystallite orientation not directly accessible by standard Rietveld analysis. XRD-CT datasets are available in Dryad [49].

All figures were created using InkScape open-source imaging and drawing software (https://inkscape.org).

3. Results

(a) PLM- and SEM-based observations

Ground sections of all investigated *Iharkutosuchus* teeth reveal a comparatively thick enamel (150–300 µm) for a crocodilian of similar size (e.g. [13,38,39,50]). Some of the premolariform and molariform cusps are slightly worn, but the majority of the enamel is well-preserved in all studied teeth. A largely columnar enamel microstructure appears to be present in cross-polarized light (c-PLM) and in some SEM images of the tooth sections (figure 1C–E), just like in the allodaposuchid crocodile and most extant crocodilians [26,39]. Other SEM images, however, reveal uniformly oriented, short and thick, prism-like structures with blunt cone-shaped ends (figure 1F–J). This prism-like layer mostly occurs on the occlusal plane of the teeth and extends from the enamel surface down to or below half of its thickness. Prism-like as these structures are, also evidenced by side-by-side comparison with mammalian enamel prisms (figure 1K), no well-defined interprismatic enamel can be observed in between them. Thus, prismatic enamel, as defined in mammals and in a few extant reptiles, such as the spiny-tailed lizard, *Uromastyx*, and a hatchling gharial (*Gavialis gangeticus*), as well as in some extinct sphenodontians [26,51–54], cannot be identified in the *Iharkutosuchus* teeth.

In the c-PLM images of all three investigated tooth types (incisiviform (figure 2A,B), premolariform (figure 2C,D) and molariform (figure 2E–G), alternating light and dark bands appear in longitudinal sections. They are organized in a sickle-shaped pattern with a broader base starting almost perpendicular to the enamel–dentine junction (EDJ) and usually tapering into a finer band that curves slightly and merges with the enamel surface at an acute angle (figure 2). These features can be observed regionally on the sides of cusps as well as on the labiolingual and mesiodistal surfaces of the teeth. Hereafter, we refer to these alternating light and dark curving bands as HSB-like pattern, recognizing its close reminiscence of HSB as it appears in human and other mammalian teeth [55,56]. By contrast to mammalian HSB, however, the HSB-like pattern in *Iharkutosuchus* teeth is characterized by a more irregular spatial distribution and a hierarchical sub-structuring depending on the scale of investigation. Band widths are resolved in c-PLM as being approx. 90 µm thick at their base at lower magnification (4×), and as thin, hairlike structures of a few µm width at higher magnification (40×) (figure 2). This hierarchical nature of the HSB-like pattern, with broader bands being subdivided into finer stripes, makes identification of band boundaries difficult. In SEM images, neither criss-crossing bundles of prisms explaining HSB in mammals nor abrupt changes in enamel crystal orientation can be observed in the largely columnar *Iharkutosuchus* enamel (figure 1C–J).

Another peculiar enamel structure apparent under c-PLM in all three types of *Iharkutosuchus* teeth corresponds to what is known as the 'wavy enamel' that has so far only been described in herbivorous dinosaurs—mostly ornithopods with elaborate mastication [26,28,31,57]. It appears as stacks of undulating waves with an alternating light and dark pattern in the successive layers that run largely parallel to the EDJ (figure 2H–J). The individual waves have an average thickness of 5.3 ± 1.6 µm. This feature is visible in both longitudinal and transverse sections of the teeth, but its spatial distribution is diverse across the different types of teeth and along the section plane. In most sections, it is present between the main and accessory cusps on the occlusal surface closer to the EDJ (figure 2H), but it may also appear as a few stacks of waves running in the middle layer, as a double layer (figure 2I), or even across the entire enamel thickness (figure 2J). Wavy enamel can regionally co-occur with —and partially overlap—the HSB-like pattern (figure 2R). A spatially less organized but similar wavy enamel feature is also discernible in the c-PLM images of allodaposuchid (figure 2N,O), theriosuchid and *Doratodon* teeth (electronic supplementary material, figure S2). Wherever observed, they occupy the entire enamel thickness in both longitudinal and cross-sections. However, unlike the wavy enamel that runs parallel to the EDJ in the teeth of *Iharkutosuchus*, these similar structures in the other studied fossil crocodilian teeth mostly run at the same acute angle as the striae of Retzius, i.e. marked growth lines deposited in multiple-day cycles during enamel formation [58]. Whereas striae of Retzius are not evident in *Iharkutosuchus* teeth, daily

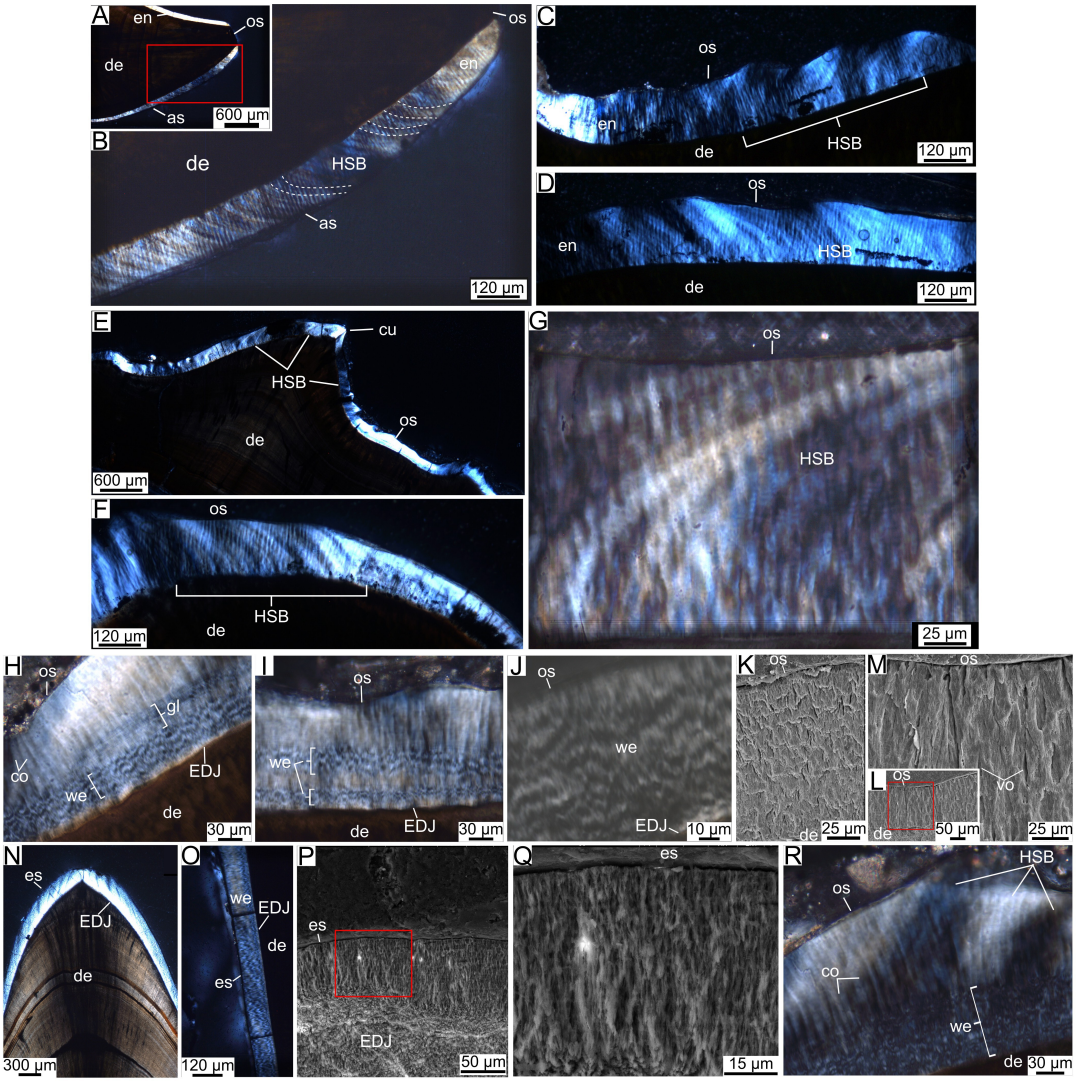

Figure 2. Hunter-Schreger band-like structures (HSB) in the tooth enamel of *Iharkutosuchus* and wavy enamel in the teeth of *Iharkutosuchus* and the sympatric allodaposuchid crocodile. HSB in longitudinally cut (A,B), incisiviform, (C,D), premolariform, and (E–G), molariform enamel appear as alternating light and dark bands under c-PLM running in a sickle-shaped pattern from the enamel–dentine junction to the outer surface of the enamel. HSB occur mostly on the anterior surface (as) up to the occlusal edge in incisiviform teeth (A,B) and on the occlusal surface in premolariform and molariform teeth running up the cusps (C–G). Note the multiple identifiable scales of bands at different magnifications. Dashed lines in (A) indicate the sickle-shaped pattern of HSB. (H–J), Wavy enamel (we) under c-PLM in *Iharkutosuchus* molariform ((H,I)) and premolariform (J) teeth organized in single (H) or multiple (I) layers or occupying the entire enamel thickness (J). Note that the waves run parallel to the enamel–dentine junction (EDJ). Daily incremental growth lines (gl) appear largely independently from wavy enamel. (K–M) SEM images of *Iharkutosuchus* molariform enamel regions with clusters of crystallites interrupted by elongate voids (vo). Red rectangle in (L) indicates magnified region in (M). (N–Q) Wavy enamel as it appears in allodaposuchid teeth under c-PLM ((N,O)) and SEM ((P,Q)). Note that the waves run at an acute angle to EDJ like the striae of Retzius, occupying the entire enamel thickness (N,O). Red rectangle in P indicates magnified region in (Q). (R) *Iharkutosuchus* molariform tooth enamel under c-PLM, demonstrating the columnar microstructure overlain by the co-occurring HSB-like and wavy enamel patterns**.** Further abbreviations as in figure 1.

incremental growth lines organized in stacks run parallel with wavy enamel layers but are manifested on a much smaller scale (approx. 1–1.5 µm zone width) and occur largely independently from wavy enamel (figure 2H).

In some SEM images of *Iharkutosuchus* teeth (figure 2K), undulating rows of poorly organized enamel crystallites resemble the so-called 'staggered crystallites' (*sensu* [26]) illustrated in the coarse wavy enamel of ornithopod dinosaurs, such as *Iguanodon*, *Hypacrosaurus* and *Saurolophus* [27,28,37]. In other samples, crystallites form thicker bundles regionally interrupted by elongated voids (figure 2L,M) that look more like the structures identified as wavy enamel in SEM images of *Anatosaurus* teeth [26]. Still, no evident spatial correlation or consistent pattern could be ascertained to link the wavy enamel appearing in c-PLM to these SEM structures in *Iharkutosuchus* teeth. Similarly, in allodaposuchid teeth, regions showing wavy enamel in c-PLM images have SEM characteristics demonstrated in diverse crocodilian enamel [e.g. 26,38,39] (figure 2P,Q), but they are also virtually indistinguishable from those identified as wavy enamel in the basal ornithopod *Changchunsaurus* (fig. 5 in [31]).

(b) HSB-like pattern explained by XRD-CT

As the structural background of the HSB-like pattern appearing in c-PLM images of the *Iharkutosuchus* teeth could not be established at a microstructural scale by SEM profiling, XRD-CT was used to probe the nanostructural level of this enigmatic phenomenon.

When HAP crystallinity is considered, relative scale factor distribution colour maps show that *Iharkutosuchus* teeth have uneven, regionally differing intensities throughout the enamel (green to red colours indicating lower to higher intensity HAP distributions in figure 3A,B,E,F and figure 4B,D). This contrasts with the strongly uniform pattern of relatively high crystallinity in the bulk of the enamel found in the teeth of the fossil allodaposuchid and the modern alligator (orange to red colours in figure 3C,D,G,H). The same difference between the tooth enamel of *Iharkutosuchus* and the other crocodilians is evident in the crystallite size distribution. In *Iharkutosuchus*, adjacent regions of larger (approx. 40–60 nm, orange to red in figure 3, yellow to red in figure 4B,D) and smaller (approx. 25–30 nm, green to yellow in figure 3, blue to green in figure 4B,D) crystallites are observed at the scale of 20–200 µm. The other crocodilians rather show a thin inner layer of smaller and a thick outer layer of larger crystallites in their enamel (figure 3G,H). Similarly, the heterogeneity in the intensity of the 300 reflection of the HAP unit cells (figure 3, electronic supplementary material, figure S3) reveals changes in the relative a-axis orientation of the HAP crystallites at the same spatial scale as the detected changes in crystallite sizes in *Iharkutosuchus*. In the HAP 300 reflection maps, finer columnar features are also visible at 8–20 µm (figure 3F,H) consistent with the columnar enamel structure appearing in SEM and c-PLM images. Although the a-axis orientation of the HAP unit cells also shows variations in the modern alligator posterior tooth (figure 3H), orientation changes in the adjacent regions are more pronounced in the *Iharkutosuchus* teeth signified by alternating red and green/blue colours, as opposed to the alternating blue and green bands seen in the alligator.

Most importantly, the spatial distribution, dimensions and hierarchical structuring of the changing intensities in HAP crystallinity (relative scale factor), crystallite size and a-axis orientation of HAP unit cells seem to match the large-scale HSB pattern identified in c-PLM images of *Iharkutosuchus* enamel (figures 3, 4, electronic supplementary material, figures S4). Even though the XRD-CT resolution in this study did not allow us to establish a relationship at the finest scale of the HSB phenomenon (figure 2D,F,G), the combination of the changes in these three identified HAP parameters appears to correlate spatially with the HSB pattern emerging at higher hierarchical levels (figure 4A–C and electronic supplementary material, figures S4). The spatial correlation that exists among the three HAP parameters in the XRD-CT is clearest in the images of the premolariform tooth. In the latter, crystallinity—and to a lesser extent, crystallite size—can be best linked to the HSB-like pattern seen under c-PLM, whereas their relationship with HAP a-axis orientation is not evident. However, as it was not possible to image the same tooth/cross-section applying these two different methods, identical matching of features between c-PLM and XRD-CT images is not to be expected.

By contrast, with similar variability in 002 reflection intensities across the studied taxa, the c-axis orientation of the HAP unit cells in *Iharkutosuchus* tooth enamel does not deviate from the pattern found in the other crocodilians (figure 3). As for lattice parameters ‘a’ and ‘c’ (electronic supplementary material, figures S5 and S6), HAP unit cell length along the a-axis (i.e. lattice parameter ‘a’) increases towards the enamel surface in the premolariform of *Iharkutosuchus* and in the posterior allodaposuchid tooth. By contrast, HAP a-axis length is mostly uniform in all other teeth, with the *Iharkutosuchus* molariform having the shortest, and the modern alligator posterior tooth the longest unit cell a-axis across the enamel (electronic supplementary material, figure S5). HAP unit cell length along the c-axis (i.e. lattice parameter ‘c’) is uniformly small throughout the enamel in all fossil teeth compared with modern alligator, in which HAP c-axis is longer in the bulk of the enamel and decreases close to the enamel surface (electronic supplementary material, figure S6). Thus, neither HAP c-axis orientation nor unit cell size seems to correlate with the HSB-like features present in *Iharkutosuchus* teeth. Furthermore, despite their appearance in the 300 reflection images, the columnar enamel units do not appear to be linked to the varying intensities of this HAP orientation parameter, which can cross columnar boundaries in a spatially uncorrelated manner. For further details on the XRD-CT observations, see the electronic supplementary material.

4. Discussion

Our study demonstrated a unique and unexpected combination of mammal-like HSB pattern and dinosaur-like wavy enamel in the teeth of the extinct herbivorous crocodilian, *Iharkutosuchus*. While c-PLM was the essential tool for primary detection of both enamel features, only XRD-CT could uncover the underlying cause of the HSB-like pattern and its important functional evolutionary implications in *Iharkutosuchus*. We also added XRD-CT to the growing list of applicable high-resolution analytical tools for deciphering the nanostructural background of adaptive characteristics in the enamel of both extant and extinct vertebrates [e.g. 39,59–64].

The evolution of vertebrate herbivory is associated with various dental adaptations to increased tooth wear caused by highly fibrous, tough plant material [14,22,65]. Such adaptations can manifest themselves at multiple scales, from anatomical to molecular, crystallite and even atomic levels [38,53,60,64,66], as also evidenced by our findings in *Iharkutosuchus*. Besides the prominent morphological and anatomical correlates of chewing [22–25], the observed combination of the HSB-like pattern and wavy enamel appears to represent much more cryptic, nano-scale adaptations to the highly specialized herbivorous diet of *Iharkutosuchus*.

The functional significance of mammalian HSB in increasing resistance to chewing-related attrition and abrasion and in mitigating crack propagation has been extensively investigated [5–9,56,61,67–72]. For instance, Lynch *et al.* [56] found that HSB

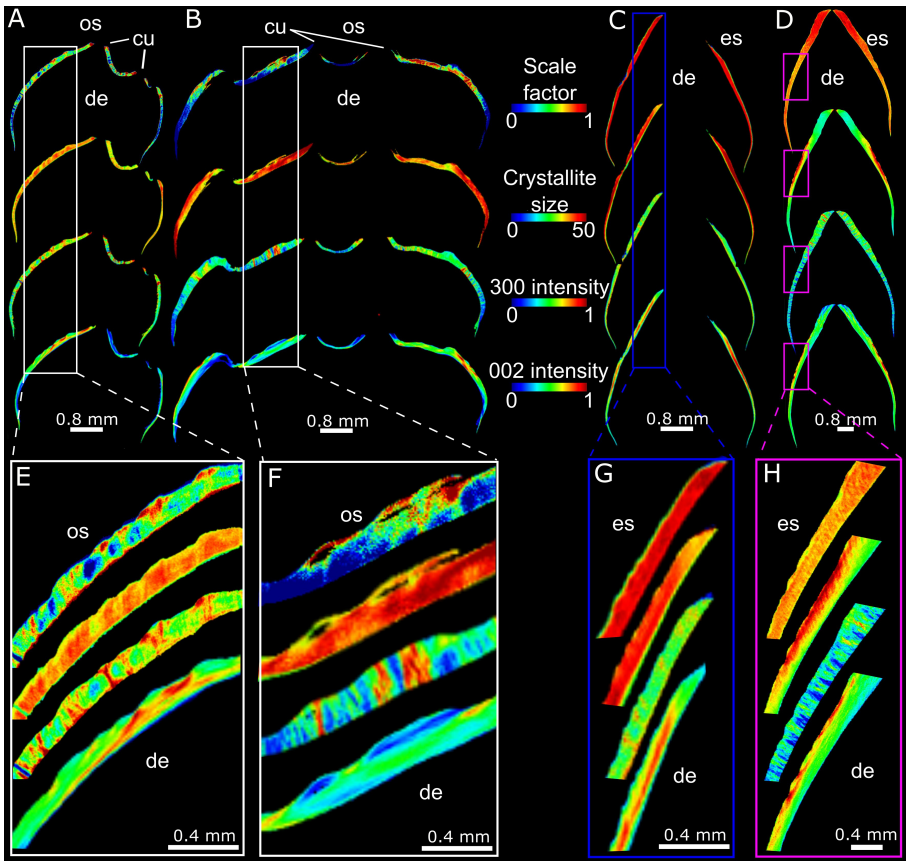

Figure 3. XRD-CT imaging of fossil and extant crocodilian teeth in longitudinal virtual section planes. (A) and (B) *Iharkutosuchus* premolariform and molariform teeth, (C) allodaposuchid posterior tooth and (D) modern alligator posterior tooth with rectangles of corresponding colour indicating magnified areas in (E–H), respectively. Four-stack images from top to bottom show intensity mapping of relative crystallinity (scale factor), crystallite size, relative a-axis orientation (300 intensity) and relative c-axis orientation (002 intensity) of HAP unit cells, respectively, in entire tooth section images ((A–D)) and a selection of magnified regions for assessing heterogeneity and spatial correlation across parameters (E–H). Note, owing to the large size of the modern alligator tooth causing parallax artefacts, only a small section of the scan highlighted in the purple rectangle delivered reliable data. Abbreviations as in figures 1 and 2.

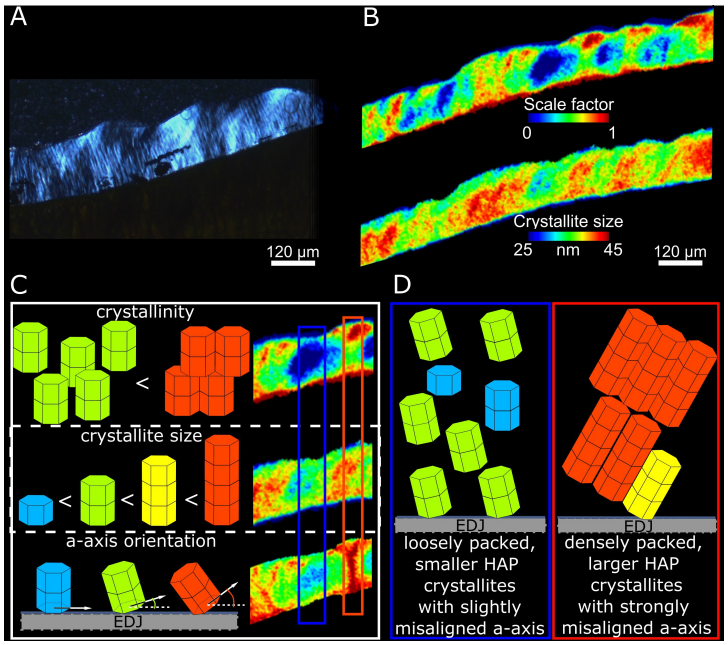

Figure 4. Matching HSB-like pattern in c-PLM images with XRD-CT images of *Iharkutosuchus* premolariform tooth enamel. (A) c-PLM image of the enamel with HSB-like pattern. (B) XRD-CT images of the enamel brought to the same scale as (A) reflect crystallinity (scale factor) and crystallite size adjusted to the range of the premolariform tooth for enhanced contrast. Note the matching intensity changes (colour differences) with the large-scale spatial distribution, orientation and size range of HSB-like dark and light bands shown in (A). (C) Crystallographic explanation of differing intensities in the three HAP parameters demonstrated in the premolariform tooth enamel and suggested here to be associated with HSB-like pattern. (D) Interpretative drawing of the HAP crystallographic background of enamel regions marked with rectangles of corresponding colour in (C). Note that the c-PLM and XRD-CT images were not taken of the same teeth and hence are not expected to show identical spatial distributions of features.

packing densities (number of HSBs/mm EDJ length) in human tooth enamel are asymmetrically distributed, being the highest in areas of greatest functional loads, like the occlusal surfaces of posterior teeth. Moreover, differences in HSB configurations, including shape, orientation, packing density or spatial distribution, have been shown to correlate well with taxon-specific dietary spectra [6,9,10,73]. Thus, we suggest that the HSB-like pattern in the enamel of the herbivorous crocodile *Iharkutosuchus* with elaborate chewing mechanism had similar functional significance in providing more resistance to highly abrasive plant material, albeit on a different structural hierarchical level.

Diversity in the appearance of HSB is considerable among different mammalian taxa with varied diet. Nevertheless, HSB in mammalian prismatic enamel are always the result of the decussation patterns defined by the various spatial arrangements of prisms. The width of individual prisms corresponds to the secretory surface of individual ameloblasts (enamel-forming cells), and thus, changing orientation of groups of prisms responsible for HSB being clearly traceable on a cellular scale [3,74–77]. Although prism-like structures are also present in the *Iharkutosuchus* enamel (figure 1F–J), they do not show any decussation pattern or other orientational changes that would correspond with the detected HSB-like features. Instead, XRD-CT revealed three HAP parameters as potential crystallographic correlates of the HSB-like pattern in *Iharkutosuchus* teeth: crystallinity, crystallite size and a-axis orientation (i.e. 300 reflection intensity) of HAP unit cells (figure 4). Although none of these parameters on their own accounts for the HSB pattern to its finest details, their combination holds the key to explain this nanostructural phenomenon in the *Iharkutosuchus* tooth enamel.

How these three parameters correlate with each other in the enamel is not entirely understood; nor is their relationship to the larger columnar enamel units of which they seem to be largely independent. In *Iharkutosuchus* teeth, higher crystallinity seems to co-occur with larger crystallites, indicating that larger crystallites can be more densely packed, while smaller crystallites are more loosely packed (figure 4C,D). However, such spatial correlation is not apparent in any of the other crocodilian teeth. Furthermore, whereas crystallinity and crystallite size both also show spatial correlation with the HAP unit cell a-axis orientation in the premolariform tooth, this trend is not apparent in the molariform tooth or in any of the other crocodilian teeth. In the *Iharkutosuchus* premolariform, lower-intensity 300 reflection areas correspond with lower crystallinity and smaller crystallite size. Thus, in this particular tooth, the a-axis of HAP unit cells is oriented closer to parallel to the tooth surface (and hence EDJ) in regions of low crystallinity and smaller crystallite size, while their misorientation increases in regions of high crystallinity and larger crystallite size (figure 4C,D). The regionally highest a-axis misalignment found in the *Iharkutosuchus* premolariform and molariform teeth (red areas in figure 3) indicates that this HAP parameter may be the main contributor to creating the HSB-like appearance under c-PLM. Even so, at this point, it cannot be conclusively determined which single parameter or combination thereof corresponds to the dark and light bands of the HSB-like pattern. Future studies could shed further light on this association by exploring how changes in these parameters influence the optical behaviour of HAP under c-PLM.

Whereas it is well-known that diagenetic processes can alter the structural and chemical characters of bioapatite [41,78–81], the only crystallographic parameter that was identical across all fossil teeth but unitedly different from modern teeth was the length of HAP unit cell along its c-axis (lattice parameter ‘c’, electronic supplementary material, figure S6). The smaller unit cell size in fossil enamel might be related to the considerably larger size of the modern alligator teeth. However, this HAP parameter is probably more prone to diagenesis-induced changes based on previous studies showing that diagenesis tends to change crystallite size-related characteristics and elemental composition rather than crystallite orientation [41,78–81]. Nevertheless, in all the other parameters, there was a considerable variability across the different samples, irrespective of their fossil or modern origin. It is noteworthy that in many parameters, the allodaposuchid enamel was more similar to the modern alligator enamel than to *Iharkutosuchus* enamel, despite the fact that these sympatric fossil crocodilians shared the same fluvial habitat with identical diagenetic and fossilization conditions [33]. This suggests that the distinct crystallographic enamel characteristics observed in *Iharkutosuchus* are intrinsic biogenic features unrelated to diagenetic alterations. Instead, they probably reflect general feeding habits and diet that were very different between *Iharkutosuchus* and allodaposuchids but very similar between allodaposuchids and modern alligators [34–36].

There is growing evidence that enamel nanostructural features are not the product of by-chance random crystallite growth but have distinct functional significance. For instance, Beniash *et al.* [61] showed that the homogeneous orientation of crystalline c-axes in interprismatic crystals *versus* the misaligned c-axes of nanocrystals in adjacent prisms, along with gradually changing c-axes orientation within a single prism, induces crack deflection in human enamel. This heterogeneity of HAP c-axis orientation among and within prisms has been considered as a toughening mechanism aiding long-term enamel resistance under great physical and chemical challenges [61]. Similarly, An *et al.* [82] found non-uniform crystal arrangement in enamel prisms (rods) and concluded that it facilitates energy dissipation, while providing a stiff and tough biocomposite material that can resist penetration and mitigate fracture propagation. This suggests that HAP heterogeneity resulting in the HSB-like pattern in *Iharkutosuchus* probably contributes to enamel toughness.

It is important to note that two studies [62,63] published PLM images of the longitudinal section of a single isolated indeterminate allodaposuchid tooth, G2-W-016, showing very similar alternating light and dark curved features in its enamel to the HSB-like pattern in *Iharkutosuchus* (fig. 1A in [62]; fig. 1H in [63]). These studies used a range of modern techniques, including synchrotron-based micro-XRD, to investigate HAP characteristics in modern and fossil crocodilian teeth. Still, this curious enamel pattern has been entirely overlooked and hence was neither recognized as HSB nor described or considered in any other way by the authors. Furthermore, both studies focused mostly on dentine characteristics with insufficient μXRD resolution to detect such fine-scale features in the enamel. Still, as the isolated G2-W-016 was assigned to an allodaposuchid crocodilian [63], the absence of similar features in our allodaposuchid teeth under c-PLM is notable. Whether the light–dark enamel pattern represents a true crystallographic optical phenomenon or other type of colouration cannot be assessed because it is not specified whether the PLM images of G2-W-016 were taken under plane-polarized or cross-polarized light. Nevertheless,

we acknowledge the resemblance and thereby the possibility that HSB-like pattern might be present in the enamel of this indeterminate crocodilian tooth and call for its further investigation in this direction.

The second enamel feature that we demonstrated in *Iharkutosuchus* teeth with presumably functional adaptative value is wavy enamel. Despite the recurring statement that it has distinct characteristics under SEM [26,37], studying our specimens and reviewing the literature, we found it difficult to identify clear and consistent SEM-based visual correlates of wavy enamel. In fact, the regional enamel microstructure of *Iharkutosuchus* with positive identification of wavy enamel under c-PLM appeared diverse, largely depending on the tooth's general preservation and their preparation for SEM imaging (naturally broken/worn/ground/ground-etched surfaces). Hoffman *et al.* [83] also noted that the arrangement of enamel crystallites in SEM images of some pseudosuchian teeth resembles those demonstrated in the wavy enamel of ornithischian dinosaurs. Yet, they could not confirm the presence of wavy enamel in c-PLM tooth images of the fossil pseudosuchians they investigated [83].

By contrast, we have demonstrated wavy enamel under c-PLM in the teeth of other fossil crocodilians known from the same locality as *Iharkutosuchus* without showing any peculiar SEM microstructural characteristics. Furthermore, the SEM features associated with the wavy enamel in the ornithopod *Changchunsaurus* [31] are indistinguishable from those found in the allodaposuchid teeth, despite the fact that the orientation of the waves under c-PLM seems to follow the striae of Retzius in allodaposuchid teeth, whereas they run parallel to EDJ in *Changchunsaurus*, just like in *Iharkutosuchus* teeth. These controversial findings also speak against a well-defined SEM-based correlate of wavy enamel. Thus, it is our conclusion that the SEM characteristics of wavy enamel can only be 'reverse-correlated' once a positive c-PLM-based identification is present and therefore cannot be used as definite wavy enamel correlates on their own. Thus far, we have found no clear and consistent demonstration that could sufficiently explain the underlying structure of wavy enamel. However, with smaller tooth samples and hence increased resolution of the focused beam, XRD-CT might be able to identify the origin of this feature in the future as well.

Wavy enamel has long been thought to be a synapomorphy of ornithopod dinosaurs exhibiting elaborate mastication [26–28,30,31,37]. However, it has recently been described in other herbivorous dinosaurs, such as stegosaurids and psittacosaurids [57]. Although stegosaurid dinosaurs are generally considered unable to chew, investigating tooth wear patterns and histology of isolated stegosaurian teeth from the Early Cretaceous of Russia, Skutschas *et al.* [57] concluded that these high-latitude stegosaurs probably performed complex oral food processing with occluding teeth and palinal jaw movement. If this reconstruction is correct, it would further support the assumed primary function of wavy enamel in reducing abrasion caused by tough plant material [37]. We suggest that the presence of wavy enamel in *Iharkutosuchus*, just like the HSB-like pattern, is indicative of high, masticatory loading regimes related to its feeding strategy. The functional significance of similar features in the other fossil crocodilians demonstrated here is a conundrum and needs further investigation.

In addition to these nano-scale adaptations, *Iharkutosuchus* also exhibits a combination of relatively thick enamel and high tooth replacement rates, corroborating its elaborate feeding habits and related dental functions. The enamel of the posterior teeth regionally reaching over 300 µm thickness is among the thickest recorded in crocodilians relative to skull length [39,50]. With an estimated replacement rate of approx. 1–4 months (Horváth, 2025, personal observation), *Iharkutosuchus* is also characterized by fast tooth replacement when compared with extant (approx. 3–6 months; [84,85]) and other fossil crocodilians living sympatrically with *Iharkutosuchus* (3–12 months; Horváth, 2025, personal observation). Even though the enamel thickness of *Iharkutosuchus* is only impressive among polyphyodont amniotes and remains in the lowest range of that observed in diphyodont mammals [50], combined with the high tooth replacement rate, it is deemed to be an efficient adaptation to chewing highly abrasive plant food. This hypothesis is supported by the comparable absolute enamel thickness and estimated tooth replacement rate in *Iharkutosuchus* and hadrosaurid dinosaurs [50,86]. Furthermore, a relatively thick enamel combined with similarly high tooth replacement rates inferred in sauropod dinosaurs [67] also implies that these distantly related archosaurian taxa shared a common evolutionary strategy to develop highly efficient herbivory. Consistent with this argument, tooth replacement rates among dinosaurs were found to be the highest in herbivores (approx. 50–80 days) and lowest in carnivores (approx. 290–780 days) [86]. Thicker enamel than found in *Iharkutosuchus* characterizes the bulbous teeth of a durophagous fossil crocodilian, *Allognathosuchus*, in which the thick enamel is considered to resist fractures and prolong the functional lifetime of the tooth ([50] & refs therein). However, in contrast to *Allognathosuchus*, tooth morphology in the distinctly heterodont *Iharkutosuchus* speaks for a herbivorous diet that is highly abrasive, but less fracture-inducing compared with durophagy. In this functional context, combining medium–high enamel thickness with high tooth replacement rate may therefore be a more advantageous herbivorous strategy than developing massive enamel proportions for deciduous teeth.

The phylogeny of amniotes clearly shows that functional adaptation-driven convergence is the most plausible explanation for the appearance of the HSB-like pattern and wavy enamel in *Iharkutosuchus* teeth. Archosauria is a monophyletic clade inclusive of the last common ancestor of crocodiles and dinosaurs, including birds, and all of its descendant clades [87–89]. Archosaurian tooth enamel essentially shows the same general microstructure of prismless units that is thought to be distinct from the typical prismatic mammalian enamel [26,37]. All the diverse manifestations of the archosaurian aprismatic enamel can be derived from these prismless units. Thus, the independent emergence of wavy enamel in different archosaurs is much less surprising than that of the mammalian-like HSB pattern in a crocodilian. The instances of parallel evolution of wavy enamel among different ornithischian groups, such as hadrosaurs and stegosaurs [57], support the notion of a comparatively simple transition from one state to another within the broad spectrum of archosaurian enamel types. In fact, the presence of wavy enamel-like patterns in the other fossil crocodilians described here suggests that the microstructural background of wavy enamel is already given in the simplest crocodilian enamel types and is probably much more widespread than previously recognized.

By contrast, HSB have thus far only been demonstrated in mammals with decussating enamel prisms. The HSB-like pattern arising from nano-scale crystallographic heterogeneity of HAP in *Iharkutosuchus* is a prime example of superficially similar

but profoundly different levels of structural adaptation. Interestingly, as shown in the HSB of fossil hyanids, the increasing proportion of hard items in the diet is linked with mosaic evolution in which microstructural adaptations precede macrostructural changes in tooth morphology [10]. Similarly conceivable is that the nanostructural characteristics of the HSB-like pattern emerged in the tooth enamel before the development of strong heterodonty in *Iharkutosuchus*.

Finally, even though we refrain from referring to the enamel of *Iharkutosuchus* teeth as prismatic owing to the apparent lack of interprismatic substance, the evolutionary history and nomenclature of prismatic enamel are still unsettled and inconclusive. The ever-growing diversity of enamel microstructure revealed in a variety of extant and fossil taxa cautions against adhering to 'carved in stone' definitions restricted to currently known and/or acknowledged enamel types and urges more focus on investigating their functional evolutionary aspects. Our findings demonstrating a 'pseudo-mammalian– dinosaurian hybrid' enamel in a fossil herbivorous crocodile further showcase a highly specialized diet as an important functional drive at each structural hierarchical level in the evolution of amniotes.

Ethics. The fossil and extant crocodilian teeth used in our study did not require any ethical approval. See further information on the origin of specimens in §2 of the main text.

Data accessibility. All necessary data are provided in §2 of the main manuscript and in the electronic supplementary material [90]. XRD-CT datasets are available in Dryad [49].

Declaration of AI use. We have not used AI-assisted technologies in creating this article.

Authors' contributions. E.P.: conceptualization, formal analysis, investigation, methodology, supervision, validation, visualization, writing—original draft, writing—review and editing; K.H.: data curation, formal analysis, investigation, methodology, visualization; S.W.T.P.: data curation, formal analysis, methodology, software, validation, visualization, writing—review and editing; O.G.: methodology, software; A.M.B.: funding acquisition, methodology, supervision.

All authors gave final approval for publication and agreed to be held accountable for the work performed therein.

Conflict of interest declaration. We declare we have no competing interests.

Funding. No funding has been received for this article.

Acknowledgements. We thank Krisztina Buczkó for the SEM access and assistance at the Hungarian Natural History Museum, Ábel Szabó for help with SEM work at Eötvös Loránd University, Júlia Katalin Török for the partial alligator tooth specimen and Attila Ősi for access to the fossil specimens. We acknowledge DESY (Hamburg, Germany), a member of the Helmholtz Association HGF, for the provision of experimental facilities. Parts of this research were carried out at beamline P07-DESY at PETRA III.

References

1. Osborn JW. 1965 The nature of the Hunter-Schreger bands in enamel. *Arch. Oral Biol*. **10**, 929–933. (doi:10.1016/0003-9969(65)90086-5)
2. Osborn JW. 1990 A 3-dimensional model to describe the relation between prism directions, parazones and diazones, and the Hunter-Schreger bands in human tooth enamel. *Arch. Oral Biol*. **35**, 1. (doi:10.1016/0003-9969(90)90065-i)
3. Hanaizumi Y, Maeda T, Takano Y. 1996 Three-dimensional arrangement of enamel prisms and their relation to the formation of Hunter-Schreger bands in dog tooth. *Cell Tissue Res*. **286**, 103–114. (doi:10.1007/s004410050679)
4. Boyde A. 1997 Microstructure of enamel. In *Dental enamel* (eds DJ Chadwick, G Cardew), pp. 18–31, vol. **205**. Chichester, UK: Ciba Found Symp, Wiley. (doi:10.1002/9780470515303)
5. von Koenigswald W. 1980 Schmelzstruktur und Morphologie in den Molaren der Arvicolidae (Rodentia). *Abh Senckenb Naturforsch Ges* **539**, 1–129.
6. von Koenigswald W, Rensberger JM, Pretzschner HU. 1987 Changes in the tooth enamel of early Paleocene mammals allowing increased diet diversity. *Nature New Biol.* **328**, 150–152. (doi:10.1038/328150a0)
7. Srivastava R, Ahmad A, Rao VR. 2022 Stress patterns in conical teeth of reptiles and mammals: experimental and finite element analyses. *Span. J. Palaeontol* **14**, 269–277. (doi:10.7203/sjp.23823)
8. Chai H, Lee JJW, Constantino PJ, Lucas PW, Lawn BR. 2009 Remarkable resilience of teeth. *Proc. Natl Acad. Sci. USA* **106**, 7289–7293. (doi:10.1073/pnas.0902466106)
9. Koenigswald WV, Holbrook LT, Rose KD. 2011 Diversity and evolution of Hunter-Schreger band configuration in tooth enamel of perissodactyl mammals. *Acta Palaeontol. Pol.* **56**, 11–32. (doi:10.4202/app.2010.0021)
10. Tseng ZJ. 2012 Connecting Hunter-Schreger band microstructure to enamel microwear features: new insights from durophagous carnivores. *Acta Palaeontol. Pol.* **57**, 473–484. (doi:10.4202/app.2011.0027)
11. Torii S, Mishima H, Suzuki K, Kozawa Y. 1995 Enamel structure of reptiles. *ACBTE* **4**, 21–26.
12. Torii S. 1998 Origin of enamel prisms and Hunter-Schreger bands in reptilian enamel. *Connect. Tissue Res.* **38**, 45–51. (doi:10.3109/03008209809017019)
13. Line SRP, Novaes PD. 2005 The development and evolution of mammalian enamel: structural and functional aspects. *Braz. J. Morphol. Sci.* **22**, 67–72.
14. Rybczynski N, Reisz RR. 2001 Earliest evidence for efficient oral processing in a terrestrial herbivore. *Nature New Biol.* **411**, 684–687. (doi:10.1038/35079567)
15. Reisz RR. 2006 Origin of dental occlusion in tetrapods: signal for terrestrial vertebrate evolution? *J. Exp. Zool. Part B Mol. Dev. Evol*. **306**, 261–277. (doi:10.1002/jez.b.21115)
16. Norman DB, Weishampel DB. 1985 Ornithopod feeding mechanisms: their bearing on the evolution of herbivory. *Am. Nat.* **126**, 151–164. (doi:10.1086/284406)
17. Erickson GM, Krick BA, Hamilton M, Bourne GR, Norell MA, Lilleodden E, Sawyer WG. 2012 Complex dental structure and wear biomechanics in hadrosaurid dinosaurs. *Science* **338**, 98–101. (doi:10.1126/science.1224495)
18. Varriale FJ. 2016 Dental microwear reveals mammal-like chewing in the neoceratopsian dinosaur *Leptoceratops gracilis*. *PeerJ* **4**, e2132. (doi:10.7717/peerj.2132)
19. Rieppel O. 2002 Feeding mechanics in Triassic stem-group sauropterygians: the anatomy of a successful invasion of Mesozoic seas. *Zool. J. Linn. Soc*. **135**, 33–63. (doi:10.1046/j.1096-3642.2002.00019.x)
20. Crofts SB, Neenan JM, Scheyer TM, Summers AP. 2017 Tooth occlusal morphology in the durophagous marine reptiles, Placodontia (Reptilia: Sauropterygia). *Paleobiology* **43**, 114–128. (doi:10.1017/pab.2016.27)
21. Pol D. 2003 New remains of *Sphagesaurus huenei* (Crocodylomorpha: Mesoeucrocodylia) from the Late Cretaceous of Brazil. *J. Vertebr. Paleontol*. **23**, 817–831. (doi:10.1671/A1015-7)

22. Ősi A. 2014 The evolution of jaw mechanism and dental function in heterodont crocodyliforms. *Hist. Biol.* **26**, 279–414. (doi:10.1080/08912963.2013.777533)
23. Ősi A, Clark JM, Weishampel DB. 2007 First report on a new basal eusuchian crocodyliform with multicusped teeth from the Upper Cretaceous (Santonian) of Hungary. *Neues Jahrb. Für Geol. Und Paläontol. Abh*. **243**, 169–177. (doi:10.1127/0077-7749/2007/0243-0169)
24. Ősi A. 2008 Cranial osteology of *Iharkutosuchus makadii*, a Late Cretaceous basal eusuchian crocodyliform from Hungary. *Neues Jahrb. Geol Paläont. Abh.* **248**, 279–299. (doi:10.1127/0077-7749/2008/0248-0279)
25. Osi A, Weishampel DB. 2009 Jaw mechanism and dental function in the late cretaceous basal eusuchian *Iharkutosuchus*. *J. Morphol.* **270**, 903–920. (doi:10.1002/jmor.10726)
26. Sander PM. 1999 *The microstructure of reptilian tooth enamel: terminology, function, and phylogeny*. vol. **38**. Munich, Germany: Pfeil.
27. Hwang SH. 2005 Phylogenetic patterns of enamel microstructure in dinosaur teeth. *J. Morphol*. **266**, 208–240. (doi:10.1002/jmor.10372)
28. Hwang SH. 2011 The evolution of dinosaur tooth enamel microstructure. *Biol. Rev. Camb. Philos. Soc*. **86**, 183–216. (doi:10.1111/j.1469-185X.2010.00142.x)
29. Heckert A, Miller-Camp J. 2013 Tooth enamel microstructure of Revueltosaurus and Krzyzanowskisaurus (Reptilia: Archosauria) from the Upper Triassic Chinle Group, USA: Implications for function, growth, and phylogeny. *Palaeontol. Electron* **16**, 1A.23. (doi:10.26879/319)
30. Godefroit P, Garcia G, Gomez B, Stein K, Cincotta A, Lefèvre U, Valentin X. 2017 Extreme tooth enlargement in a new Late Cretaceous rhabdodontid dinosaur from Southern France. *Sci. Rep*. **7**, 13098. (doi:10.1038/s41598-017-13160-2)
31. Chen J, LeBlanc ARH, Jin L, Huang T, Reisz RR. 2018 Tooth development, histology, and enamel microstructure in *Changchunsaurus parvus*: implications for dental evolution in ornithopod dinosaurs. *PLoS One* **13**, e0205206. (doi:10.1371/journal.pone.0205206)
32. Rabi M, Sebők N. 2015 A revised Eurogondwana model: Late Cretaceous notosuchian crocodyliforms and other vertebrate taxa suggest the retention of episodic faunal links between Europe and Gondwana during most of the Cretaceous. *Gondwana Res.* **28**, 1197–1211. (doi:10.1016/j.gr.2014.09.015)
33. Botfalvai G, Haas J, Bodor ER, Mindszenty A, Ősi A. 2016 Facies architecture and palaeoenvironmental implications of the upper Cretaceous (Santonian) Csehbánya formation at the Iharkút vertebrate locality (Bakony Mountains, Northwestern Hungary). *Palaeogeogr. Palaeoclimatol. Palaeoecol.* **441**, 659–678. (doi:10.1016/j.palaeo.2015.10.018)
34. Delfino M, Codrea V, Folie A, Dica P, Godefroit P, Smith T. 2008 A complete skull of *Allodaposuchus precedens* Nopcsa, 1928 (Eusuchia) and a reassessment of the morphology of the taxon based on the Romanian remains. *J. Vertebr. Paleontol*. **28**, 111–122. (doi:10.1671/0272-4634(2008)28[111:acsoap]2.0.co;2)
35. Blanco A, Puértolas-Pascual E, Marmi J, Vila B, Sellés AG. 2014 *Allodaposuchus palustris* sp. nov. from the Upper Cretaceous of Fumanya (South-Eastern Pyrenees, Iberian Peninsula): systematics, palaeoecology and palaeobiogeography of the enigmatic allodaposuchian crocodylians. *PLoS One* **9**, e115837. (doi:10.1371/journal.pone.0115837)
36. Csiki-Sava Z, Buffetaut E, Ősi A, Pereda-Suberbiola X, Brusatte SL. 2015 Island life in the Cretaceous - faunal composition, biogeography, evolution, and extinction of land-living vertebrates on the Late Cretaceous European archipelago. *Zookeys* **469**, 1–161. (doi:10.3897/zookeys.469.8439)
37. Sander PM. 2000 Prismless enamel in amniotes: terminology, function, and evolution. In *Development, function and evolution of teeth* (eds MF Teaford, MM Smith, MW Ferguson), pp. 92–106. Cambridge, UK: Cambridge University Press. (doi:10.1017/CBO9780511542626.007)
38. Dauphin Y, Williams CT. 2008 Chemical composition of enamel and dentine in modern reptile teeth. *Mineral. Mag* **72**, 247–250. (doi:10.1180/minmag.2008.072.1.247)
39. Enax J, Fabritius HO, Rack A, Prymak O, Raabe D, Epple M. 2013 Characterization of crocodile teeth: correlation of composition, microstructure, and hardness. *J. Struct. Biol.* **184**, 155–163. (doi:10.1016/j.jsb.2013.09.018)
40. Prondvai E, Godefroit P, Adriaens D, Hu DY. 2018 Intraskeletal histovariability, allometric growth patterns, and their functional implications in bird-like dinosaurs. *Sci. Rep*. **8**, 258. (doi:10.1038/s41598-017-18218-9)
41. Mürer FK, Sanchez S, Álvarez-Murga M, Di Michiel M, Pfeiffer F, Bech M, Breiby DW. 2018 3D Maps of mineral composition and hydroxyapatite orientation in fossil bone samples obtained by X-ray diffraction computed tomography. *Sci. Rep.* **8**, 10052. (doi:10.1038/s41598-018-28269-1)
42. Combes C, Cazalbou S, Rey C. 2016 Apatite biominerals. *Minerals* **6**, 34. (doi:10.3390/min6020034)
43. Egan CK, Jacques SDM, Di Michiel M, Cai B, Zandbergen MW, Lee PD, Beale AM, Cernik RJ. 2013 Non-invasive imaging of the crystalline structure within a human tooth. *Acta Biomater.* **9**, 8337–8345. (doi:10.1016/j.actbio.2013.06.018)
44. Leung N, Harper RA, Zhu B, Bartlett SA, Ignatyev K, Shelton RM, Landini G, Sui T. 2025 3D Multi-modal Imaging of demineralised dentine using combined synchrotron µ-XRD-CT and STXM-CT. *J. Struct. Biol*. **217**, 108208. (doi:10.1016/j.jsb.2025.108208)
45. Harding G, Kosanetzky J, Neitzel U. 1987 X-ray diffraction computed tomography. *Med. Phys*. **14**, 515–525. (doi:10.1118/1.596063)
46. Ashiotis G, Deschildre A, Nawaz Z, Wright JP, Karkoulis D, Picca FE, Kieffer J. 2015 The fast azimuthal integration Python library: *pyFAI*. *J. Appl. Crystallogr*. **48**, 510–519. (doi:10.1107/s1600576715004306)
47. Dong H, Jacques SDM, Papoutsellis E, Beale AM, Vamvakeros A. 2025 BeamStop: a software for analysing chemical imaging and tomography data. *ChemXiv*. (doi:10.26434/chemrxiv-2025-m1v5v)
48. Coelho AA. 2018 TOPAS and TOPAS-Academic: an optimization program integrating computer algebra and crystallographic objects written in C++. *J. Appl. Crystallogr.* **51**, 210–218. (doi:10.1107/S1600576718000183)
49. Price SWT, Prondvai E, Horváth K, Gutowski O, Beale A. 2025 Data from: United by chewing: Hunter-Schreger band-like pattern and wavy enamel in a fossil crocodile suggest functional convergence with mammals and dinosaurs. Dryad Digital Repository (doi:10.5061/dryad.6q573n6c9)
50. Sellers KC, Schmiegelow AB, Holliday CM. 2019 The significance of enamel thickness in the teeth of *Alligator mississippiensis* and its diversity among crocodyliforms. *J. Zool.* **309**, 172–181. (doi:10.1111/jzo.12707)
51. Cooper JS, Poole DFG. 1973 The dentition and dental tissues of the agamid lizard, *Uromastyx*. *J. Zool.* **169**, 85–100. (doi:10.1111/j.1469-7998.1973.tb04654.x)
52. Sahni A. 1987 Evolutionary aspects of reptilian and mammalian enamel structure. *Scanning Microsc.* **1**, 1903–1912. https://digitalcommons.usu.edu/microscopy/vol1/iss4/38/
53. Diekwisch TGH, Jin T, Wang X, Ito Y, Schmidt M, Druzinsky R, Yamane A, Luan X. 2009 Amelogenin evolution and tetrapod enamel structure. *Front. Oral Biol.* **13**, 74–79. (doi:10.1159/000242395)
54. LeBlanc ARH, Apesteguía S, Larsson HCE, Caldwell MW. 2020 Unique tooth morphology and prismatic enamel in Late Cretaceous Sphenodontians from Argentina. *Curr. Biol.* **30**, 1755–1761. (doi:10.1016/j.cub.2020.02.071)
55. Mortell JF Jr, Peyton FA. 1956 Observations of Hunter-Schreger bands. *J. Dent. Res.* **35**, 804–823. (doi:10.1177/00220345560350052201)
56. Lynch CD, O'Sullivan VR, Dockery P, McGillycuddy CT, Sloan AJ. 2010 Hunter-Schreger band patterns in human tooth enamel. *J. Anat.* **217**, 106–115. (doi:10.1111/j.1469-7580.2010.01255.x)
57. Skutschas PP *et al*. 2021 Wear patterns and dental functioning in an Early Cretaceous stegosaur from Yakutia, Eastern Russia. *PLoS One* **16**, e0248163. (doi:10.1371/journal.pone.0248163)
58. Line SRP. 2000 Incremental markings of enamel in ectothermal vertebrates. *Arch. Oral Biol*. **45**, 363–368. (doi:10.1016/s0003-9969(00)00005-4)

59. Jones MEH *et al*. 2018 Neutron scanning reveals unexpected complexity in the enamel thickness of an herbivorous Jurassic reptile. *J. R. Soc. Interface* **15**, 20180039. (doi:10.1098/rsif.2018.0039)
60. Koblischka-Veneva A, Koblischka MR, Schmauch J, Hannig M. 2018 Human dental enamel: a natural nanotechnology masterpiece investigated by TEM and t-EBSD. *Nano Res.* **11**, 3911–3921. (doi:10.1007/s12274-018-1968-1)
61. Beniash E, Stifler CA, Sun CY, Jung GS, Qin Z, Buehler MJ, Gilbert P. 2019 The hidden structure of human enamel. *Nat. Commun.* **10**, 4383. (doi:10.1038/s41467-019-12185-7)
62. Vallcorba O, Canillas M, Audije-Gil J, Barroso-Barcenilla F, González-Martín A, Molera J, Rodríguez MA, Cambra-Moo O. 2021 Synchrotron X-ray microdiffraction to study dental structures in Cretaceous crocodylomorphs. *Cretac. Res*. **128**, 104960. (doi:10.1016/j.cretres.2021.104960)
63. Audije-gil J *et al*. 2022 Going deeper into modern and fossil crocodilian tooth microanatomy: what can be inferred of palaeoenvironment and taphonomy from histochemical analyses? *Riv. Ital. Dl Paleontol. E Stratigr* **128**, 539–557. (doi:10.54103/2039-4942/15607)
64. Besnard C, Marie A, Sasidharan S, Harper RA, Shelton RM, Landini G, Korsunsky AM. 2023 Synchrotron X-ray studies of the structural and functional hierarchies in mineralised human dental enamel: a state-of-the-art review. *Dent. J.* **11**, 98. (doi:10.3390/dj11040098)
65. D'Emic MD, Whitlock JA, Smith KM, Fisher DC, Wilson JA. 2013 Evolution of high tooth replacement rates in sauropod dinosaurs. *PLoS One* **8**, e69235. (doi:10.1371/journal.pone.0069235)
66. DeRocher KA *et al*. 2020 Chemical gradients in human enamel crystallites. *Nature* **583**, 66–71. (doi:10.1038/s41586-020-2433-3)
67. Rensberger JM. 1997 Mechanical adaptation in enamel. In *Tooth enamel microstructure* (eds W Koenigswald, MP Sander), pp. 237–257, 1st edn. London, UK: CRC Press. (doi:10.1201/9781003077930-13)
68. Lynch CD, O'sullivan VR, Dockery P, McGillycuddy CT, Rees JS, Sloan AJ. 2011 Hunter-Schreger Band patterns and their implications for clinical dentistry. *J. Oral Rehabil*. **38**, 359–365. (doi:10.1111/j.1365-2842.2010.02162.x)
69. Yilmaz ED, Schneider GA, Swain MV. 2015 Influence of structural hierarchy on the fracture behaviour of tooth enamel. *Phil. Trans. R. Soc. A.* **373**, 20140130. (doi:10.1098/rsta.2014.0130)
70. Pro JW, Barthelat F. 2019 Discrete element models of tooth enamel, a complex three-dimensional biological composite. *Acta Biomater.* **94**, 536–552. (doi:10.1016/j.actbio.2019.04.058)
71. Hogg RT, Elokda A. 2021 Quantification of enamel decussation in gracile and robust capuchins (*Cebus, Sapajus* , Cebidae, Platyrrhini). *Am. J. Primatol*. **83**, e23246. (doi:10.1002/ajp.23246)
72. Yang D, Bharatiya M, Grine FE. 2022 Hunter-Schreger Band configuration in human molars reveals more decussation in the lateral enamel of 'functional' cusps than 'guiding' cusps. *Arch. Oral Biol*. **142**, 105524. (doi:10.1016/j.archoralbio.2022.105524)
73. Wilmers J, Bargmann S. 2020 Nature's design solutions in dental enamel: uniting high strength and extreme damage resistance. *Acta Biomater.* **107**, 1–24. (doi:10.1016/j.actbio.2020.02.019)
74. Hanaizumi Y, Shimokobe H, Wakita M. 1994 The three-dimensional structure of Tomes' processes and their relationship to arrangement of enamel prism in dog teeth. *Arch. Histol. Cytol.* **57**, 129–138. (doi:10.1679/aohc.57.129)
75. Hanaizumi Y, Yokota R, Domon T, Wakita M, Kozawa Y. 2010 The initial process of enamel prism arrangement and its relation to the Hunter-Schreger bands in dog teeth. *Arch. Histol. Cytol.* **73**, 23–36. (doi:10.1679/aohc.73.23)
76. White SN, Luo W, Paine ML, Fong H, Sarikaya M, Snead ML. 2001 Biological organization of hydroxyapatite crystallites into a fibrous continuum toughens and controls anisotropy in human enamel. *J. Dent. Res.* **80**, 321–326. (doi:10.1177/00220345010800010501)
77. Cox BN. 2013 How the tooth got its stripes: patterning via strain-cued motility. *J. R. Soc. Interface* **10**, 20130266. (doi:10.1098/rsif.2013.0266)
78. Kohn MJ, Schoeninger MJ, Barker WW. 1999 Altered states: effects of diagenesis on fossil tooth chemistry. *Geochim. Cosmochim. Acta* **63**, 2737–2747. (doi:10.1016/S0016-7037(99)00208-2)
79. Keenan SW, Engel AS, Roy A, Lisa Bovenkamp-Langlois G. 2015 Evaluating the consequences of diagenesis and fossilization on bioapatite lattice structure and composition. *Chem. Geol*. **413**, 18–27. (doi:10.1016/j.chemgeo.2015.08.005)
80. Ferretti A, Medici L, Savioli M, Mascia MT, Malferrari D. 2021 Dead, fossil or alive: Bioapatite diagenesis and fossilization. *Palaeogeogr. Palaeoclimatol. Palaeoecol.* **579**, 110608. (doi:10.1016/j.palaeo.2021.110608)
81. Dauphin Y. 2022 Vertebrate taphonomy and diagenesis: implications of structural and compositional alterations of phosphate biominerals. *Minerals* **12**, 180. (doi:10.3390/min12020180)
82. An B, Wang R, Zhang D. 2012 Role of crystal arrangement on the mechanical performance of enamel. *Acta Biomater*. **8**, 3784–3793. (doi:10.1016/j.actbio.2012.06.026)
83. Hoffman DK, Miller-Camp JA, Heckert AB. 2021 Tooth enamel microstructure in North American Phytosauria (Diapsida: Archosauriformes): implications for biogeography and ecology of a Late Triassic clade of crocodylian-like predators. *Palaeontol. Electron.* **24**, a32. (doi:10.26879/1162)
84. Erickson GM. 1996 Daily deposition of dentine in juvenile *Alligator* and assessment of tooth replacement rates using incremental line counts. *J. Morphol*. **228**, 189–194. (doi:10.1002/(SICI)1097-4687(199605)228:2<189::AID-JMOR7>3.0.CO;2-0)
85. Finger JW Jr, Thomson PC, Isberg SR. 2019 A pilot study to understand tooth replacement in near-harvest farmed saltwater crocodiles (*Crocodylus porosus*): implications for blemish induction. *Aquaculture* **504**, 102–106. (doi:10.1016/j.aquaculture.2019.01.060)
86. Erickson GM. 1996 Incremental lines of von Ebner in dinosaurs and the assessment of tooth replacement rates using growth line counts. *Proc. Natl Acad. Sci. USA* **93**, 14623–14627. (doi:10.1073/pnas.93.25.14623)
87. Sereno PC. 1991 Basal archosaurs: phylogenetic relationships and functional implications. *J. Vertebr. Paleontol.* **2**, 1–53. (doi:10.1080/02724634.1991.10011426)
88. Benton MJ. 2004 *Vertebrate paleontology*, 3rd edn. Oxford, UK: Blackwell Science.
89. Nesbitt SJ. 2011 The early evolution of archosaurs: relationships and the origin of major clades. *Bull. Am. Mus. Nat. Hist* **352**, 1–292. (doi:10.1206/352.1)
90. Prondvai E, Horváth K, Price SW, Gutowski O, Beale AM. 2025 Supplementary material from: United by chewing: Hunter-Schreger band-like pattern and wavy enamel in a fossil crocodile suggest functional convergence with mammals and dinosaurs. Figshare. (doi:10.6084/m9.figshare.c.8210474)